5-2014

The Role of Phosphorylation in Myosin Driven Organelle Movements in Arabidopsis thaliana

Peter Andrew Duden
pduden@utk.edu

The Role of Phosphorylation in Myosin Driven Organelle Movements in *Arabidopsis thaliana*

By

PETER DUDEN
Advisor: Andreas Nebenführ
May 2014

An Honors Thesis

Presented to the Faculty of the

Department of Biochemistry and Cellular and Molecular Biology

& the Chancellor's Honors Program

University of Tennessee, Knoxville

In Partial Fulfillment of the
Requirements for the Degree of
Bachelor of Science

ABSTRACT

Cytoplasmic streaming in plant cells is the continuous flow of cytoplasm and organelles throughout the cell, with the first observation of cytoplasmic streaming being published in 1774. The root hairs of *Arabidopsis thaliana* provide excellent cells to study this phenomenon due to their rapid polarized growth at the root hair tip, which requires a continuous supply of building blocks for cell wall and plasma membrane synthesis. Experimentation with this model system and animal based models have demonstrated that the cytoskeleton is a main mechanistic component of cytoplasmic streaming. Research now supports that the interaction of myosin XI motor proteins with organelles while sliding along actin filaments generates the motive force that is observed as cytoplasmic streaming in plants. From this, a key topic of interest is how myosin driven organelle movement is regulated. Our research focuses on whether phosphorylation affects the regulation of myosin XI motor proteins. Specifically, the goal of our research is to determine the presence of regulation of myosin XI motors by phosphorylation, and whether phosphorylation has a significant effect on cytoplasmic streaming.

The presence of phosphorylation regulation on myosin XI trafficking was determined with kinase and phosphatase inhibitors on myosin and organelle localization and movement in *Arabidopsis thaliana*. We observed few significant increases or decreases in movements above 0.5 µm/s after addition of inhibitors in myosin isoform MYA1 and fluorescently tagged organelles. The localization of MYA1 and organelles also remained unchanged. However, the percentage of movements above 0.5 µm/s became altered, indicating that phosphorylation affects organelle trafficking through the number of actively moving organelles. Whether the proportion of streaming velocities increased or decreased by kinase and phosphatase inhibitors depended on

the organelle observed, indicating the effects of phosphorylation may vary among different types of organelles.

TABLE OF CONTENTS

INTRODUCTION

Cytoplasmic streaming in plants is a visible phenomenon conserved among all cells

Cytoplasmic streaming distributes organelles, metabolites, and cytoplasm throughout the cell and depends on a motive force to function. Although cytosol movement is present in plant and animal cells, the cytoplasmic streaming in the former is more prominent as a result of an inability to change shape or position from their cell wall (Shimmen, 2007). The velocity of cytosol movement varies over a great range, with the average speed being multiple micrometers per second. Various types of cytoplasmic streaming patterns have been observed including agitation, circulation, rotation, fountain streaming, cytoplasmic streaming along predictable tracks, and tidal streaming (Kamiya, 1959). Through these patterns, cytoplasmic streaming is thought to facilitate the growth, cell differentiation, and polarization that passive diffusion could not achieve. Because of its major implications in growth, a significant amount of research is aimed to discover what creates cytoplasmic streaming's motive force.

Figure 1. ***A. thaliana*** **root and root hairs.** From the root tip upward, the root hairs develop from bulges budding out to lengths of 1 mm. Once growth is complete, the central vacuole can occupy the entire length of the cell. Figure: Diet et al. 2006.

Root hairs are ideal to study cytoplasmic streaming

The root hairs of *A. thaliana* provide an excellent model to study cytoplasmic streaming, as they are unicellular, require significant cytoplasmic streaming as a result of fast polarized growth (greater than 1 μm/min), and are positioned away from the main root for clear observation (Figure 1, Park and Nebenführ 2011).

Functionally, root hairs increase the surface area of the root for optimal absorption of water and nutrients from soil. Mutations of root hair formation are not lethal to *A. thaliana* development, which allows knockout lines to be created and observed. Inhibitors and probes are also easily facilitated due to the lack of a cuticle, which would be an additional barrier. Other similar model cells utilized to study cytoplasmic streaming include pollen tubes from flowering plants and algal cells from *Chara* species.

Myosin motor proteins have significant impacts in cell phenomena and growth

When cytosol from plant cells was isolated and observed to be insufficient in generating motive force alone, a molecular motor was hypothesized as the possible source (Kamiya and Kuroda, 1956). Myosins, known as ATP-dependent motor proteins, are now most supported to generate cytoplasmic streaming. The myosin superfamily is already known to be components of other important cellular processes, including mammalian muscle contraction and coordination of the mitotic spindle in metaphase (Sellers, 2000). Structurally, myosin motor proteins can exist as monomers or dimers, and possess conserved regions that include the following: a motor head domain binding ATP for hydrolysis (Tominaga et al., 2003); a globular tail domain that carries cellular cargo and has a CC (coiled coiled) region typical of dimers (Li and

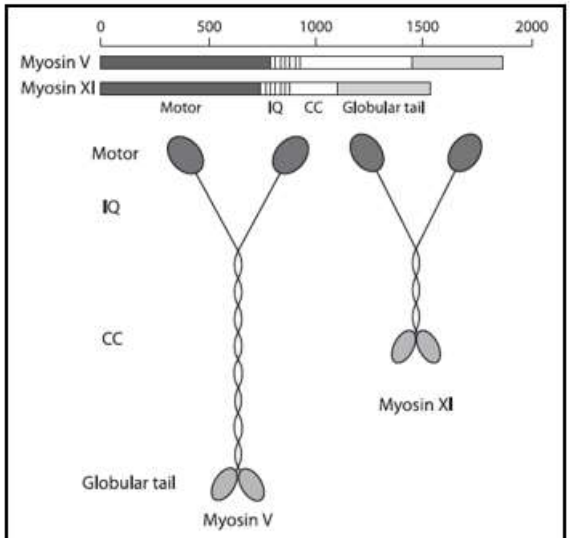

Figure 2. **Structure of myosin V and XI.** The most highly conserved region for all classes of myosin is the motor head domain. Differences in the IQ motif and CC domain vary, with the globular tail being the most diverse among each class. Myosin V, well characterized in mammalian cells, is structurally similar to myosin XI in plants, which may lead to similar roles in cell function and regulation. Figure: Li and Nebenführ, 2008.

Nebenführ, 2008); and a neck domain composed of an IQ (isoleucine and glutamine) motif that may interact with CaM (calmodulin) (Tominaga et al., 2012; Figure 2). With each functioning as a molecular motor through ATP hydrolysis, there are 35 known myosin classes in eukaryotes (Odronitz and Kollmar, 2007). Of these classes, VIII and XI myosins are found in plants and XI plays an active role in cytoplasmic streaming (Odronitz and Kollmar, 2007; Shimmen, 2007).

Acto-myosin systems contribute to cytoplasmic streaming through organelle trafficking

Myosin motors are in close interaction with actin filaments, which function as tracks that run longitudinally across the cell. Observations of myosin sliding on actin filament bundles with chloroplast cargo first indicated that an acto-myosin system was present in cytoplasmic streaming (Kamiya and Kuroda, 1956; Higashi-Fugime, 1980). F-actin had been thought to have an infrastructural role for organelle trafficking, and subsequent research later showed inhibition of F-actin bundles halted cytoplasmic streaming in root hairs (Miller et al., 1999). Further support of the acto-myosin system causing cytoplasmic streaming includes research that inhibition of plant myosin XI results in halted cytoplasmic streaming, and that altering the speed of myosin motor proteins directly alters the speed of cytoplasmic streaming, with plant size being ultimately affected (Tominaga et al., 2000; Tominaga et al., 2013).

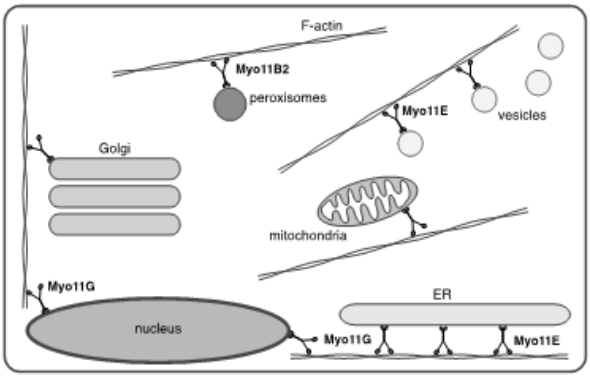

Figure 3. **Predicted organelle trafficking of myosin XI.** Nuclei, peroxisomes, and vesicles have been directly demonstrated to be dependent on myosin XI movement, with the rest supported by transient expression. The myosin XI subtype involved in organelle movement is listed. Figure: Madison and Nebenführ, 2013.

Research on myosin XI has supported its role in prominent organelle trafficking and cytoplasmic streaming. In our lab, mutations of myosin XI result in shorter root hairs, indicating

myosin XI is needed for cell growth (Vidali et al., 2010; Park and Nebenführ, 2011). Epitopes of anti-myosin antibodies on vesicular organelles, identified through immunohistochemistry, have also demonstrated myosin XI's role in membrane trafficking (Yokota et al., 2001). Notably, myosin XI is the fastest known myosin motor class, with one subtype processively moving along actin at 60 µm/s due to its high rate of ATP hydrolysis and large displacement in each step (Tominaga et al., 2003). Specifically, myosin XI's displacement has been analyzed to be 35 nm, which is the same length as a half-helical turn of actin filaments and allows the motor to move its cargo without revolving (Tominaga et al., 2003). Myosin XI is clearly optimal for carrying organelles across a growing cell, with many organelle interactions being discovered in recent research (Figure 3).

Regulation of class XI myosin motor-cargo interactions may be based on phosphorylation

The factors that regulate myosin activity are an important area of interest; however, mechanisms that regulate the acto-myosin system for class XI myosins are still unknown. Previous research concerning the regulation of myosins have centered on actin binding proteins facilitating the assembly and disassembly of actin bundles, the effect of pH and temperature on myosin protein interactions, and phosphorylation in *Chara* cells (Morimatsu et al., 2002; Kwak et al., 2005; Ishida et al., 2008). Class V myosins, which have many conserved structures to class XI myosins, contain a regulatory region in their neck domain that is affected by phosphorylation (Redowicz, 2001; Figure 2). Specifically, phosphorylation on the heavy chain during mitosis inactivates myosin V organelle trafficking, allowing the cell to

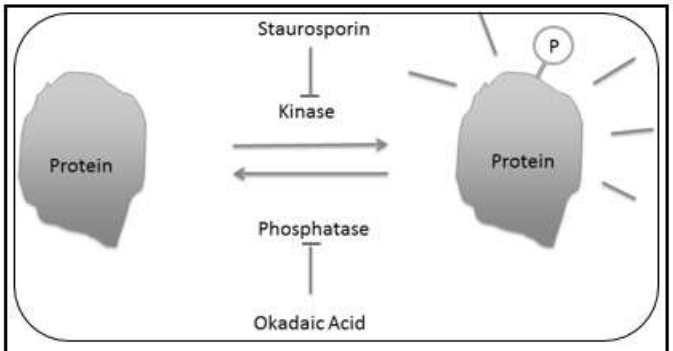

Figure 4. **Basis for kinase and phosphatase inhibitors.** Administration of staurosporin results in unphosphorylated protein, while administration of okadaic acid leads to phosphorylated protein.

cleave into two (Rogers et al., 1999). Class II myosins in muscle are also regulated by phosphorylation through a regulatory domain on their light chains, which is phosphorylated by either non-specific kinases or a specific light chain kinase (Trybus, 1991). As such, plant myosin XI may also be regulated by phosphorylation.

In this experiment, inhibitors of phosphorylation were utilized in order to observe the regulatory role phosphorylation has on organelle velocities carried by myosin XI. The kinase inhibitor staurosporin and the phosphatase inhibitor okadaic acid were administered, effectively fixing myosin XI motor proteins in unphosphorylated or phosphorylated states respectively (Figure 4). Velocities of organelles from timelapses were analyzed to determine the effects of phosphorylation on myosin XI.

MATERIALS AND METHODS

Plant Lines

Three *A. thaliana* seed lines were used for the experiment. All single YFP and CFP markers for MYA1 and RabA4b seed lines were connected to the N terminus of the tagged protein and were created in our lab by Eunsook Park. A triple organelle marker (TOM) was also utilized, containing peroxisome-CFP, Mitochondria-YFP, and Golgi-mCherry in one binary vector. Specifically, TOM was created through combining Golgi-mCherry with Mitochondria-YFP and Peroxisome-CFP by individual 35S promoters in the binary vector pFGC19. Both the single and triple organelle markers were transformed with *Agrobacterium tumefaciens* into wild type *Arabidopsis thaliana* (Weigel and Glazebrook, 2002). Our lab previously isolated several T1 plants per

genotype, with observations of organelles in T2 plants.

Seed preparation and growth conditions

Seedlings were sterilized in solution composed of 30% bleach, 0.1% Triton X-100, and distilled water for eight minutes. Sterilization solution was replaced three times with 1000 microliters of distilled water and exposed to cold conditions (4° C) for twenty-four hours.

Seedlings were then placed individually on vertical plates, with approximately 10 seeds per plate. The vertical plates were formed with one-fourth strength Murashige and Skoog Basal Salt Mixture nutrient solution (MSNS) comprised of one liter of sterile water with 1.08 g MS salts, 10 g sucrose, 2 g phytagel, and adjusted to a pH of 6.0 with 0.1 M KOH. Plates were then placed in an incubator with long day conditions (22° C, 16 h daylight and 8 h dark) for 5 days to germinate and grow.

Fluorescence Microscopy

For capturing time-lapse images of organelle markers from each of the grown seedlings, an Axiovert 200M inverted microscope (Zeiss, http://www.zeiss.com) with filters CFP, YFP, and RFP (filter set: 52017, YFP/CFP or 24002, CFP/YFP/mCherry, Chroma, http://www.chroma.com) was used in combination with a Hamamatsu Orca ER digital camera (Hamamatsu Photonics, http://www.hamamatsu.com) controlled with OpenLab software (Improvision, http://www.improvision.com). Signals were checked on the seedling with the 20X objective before switching to the 63X oil immersion objective for imaging. Seedlings were observed individually by first pipetting 100 microliters of ¼ MS medium on a large cover glass and then placing the seedling in the medium. A cover slip was pasted with vacuum grease on two sides and gently placed over the

seedling to create an observation chamber. The observation chamber with the seedling was then placed on the microscope.

Obtaining Timelapses and Pictures

Once a root hair was found on 63X objective with optimal cytoplasmic streaming and growth, a one minute timelapse with one or two pictures per second were taken. After the timelapse, pictures from five different focal planes of the root hair were also taken. To obtain inhibitor data, three aliquots of 100 microliters of dimethyl sulfoxide (DMSO; 1% in MSNS), staurosporin (200 nM in MSNS and 1% DMSO), or okadaic acid (200 nM in MSNS and 1% DMSO) were pipetted to replace the original medium inside the observation chamber. The medium was removed by allowing a piece of paper towel to contact the observation chamber on the opposite side of where the inhibitor or control solution was being added, allowing the medium to enter the paper as the inhibitor pushed the medium out of the observation chamber. Care was taken to not move the coverslip or move the lens out of sight of the root hair while displacing the medium with inhibitor. After ten minutes to allow the inhibitor to take effect, another one minute timelapses and five pictures at different planes of the root hair were taken. Data was discarded if the root hair was damaged or burst at the tip after administration of inhibitor.

Quantitative analysis of MYA1, RabA4b, and TOM movements

Timelapse data was put through a 'Subtract background' macro in ImageJ software (NIH, http://rsbweb.nih.gov/ij/) to eliminate background signal. Organelle signals in timelapses were then tracked using the ImageJ plugin 'Particle Detector and Tracker' (Sbalzarini and Koumoutsakos, 2005). Radius, cutoff, and percentile parameters were adjusted until the tracker

identified most signals correctly and the least amount of tracks were reported. The link range was set to 1 to prevent the tracker from skipping to other signals. Optimization was achieved through adjusting each variable by increments and comparing each result. Additionally, the data obtained from default values of the plugin were compared with data optimized to contain the least number of tracks in order to ensure the sum of the number of total steps were similar between both analyses. A final macro was run to detect likely false lining assignments from the tracking plugin and remove them from the list. The organelles tracked by the plugin converted the data to velocities and the number of unique tracks present. Statistical analysis was done using Prism software. A minimum of 4 root hairs for each treatment and organelle were obtained for analysis.

Pictures from different planes were combined into one image and compared before and after administration of inhibitor or control. Images were also contrast enhanced in order to more accurately identify signals.

RESULTS

Organelle Localization

Rationale: *If phosphorylation regulates movement, then changes in phosphorylation may lead to alteration in the distribution of moving organelles.*

Individual root hairs were observed pre- and post-treatment for kinase and phosphatase inhibitors in order to test the above rationale. Myosin MYA1 localization was across the whole root hair, with MYA1 signaling being most concentrated at the root hair tip (Figure 5). RabA4b vesicle localization had a much more diffuse signal, leading to a fluid-like motion centered

around the root hair tip (Figure 5). The signal from Golgi bodies were observed as globular with diffuse fluorescent spread throughout the entire root hair (Figure 5). Last, peroxisome signal movement could be characterized as large beads moving in a linear pattern. Peroxisome signals were not as abundant as MYA1, RabA4b, or Golgi bodies, but were larger in spot size (Figure 5). All organelles had no localization change, with small differences in signal size or localization deemed insignificant.

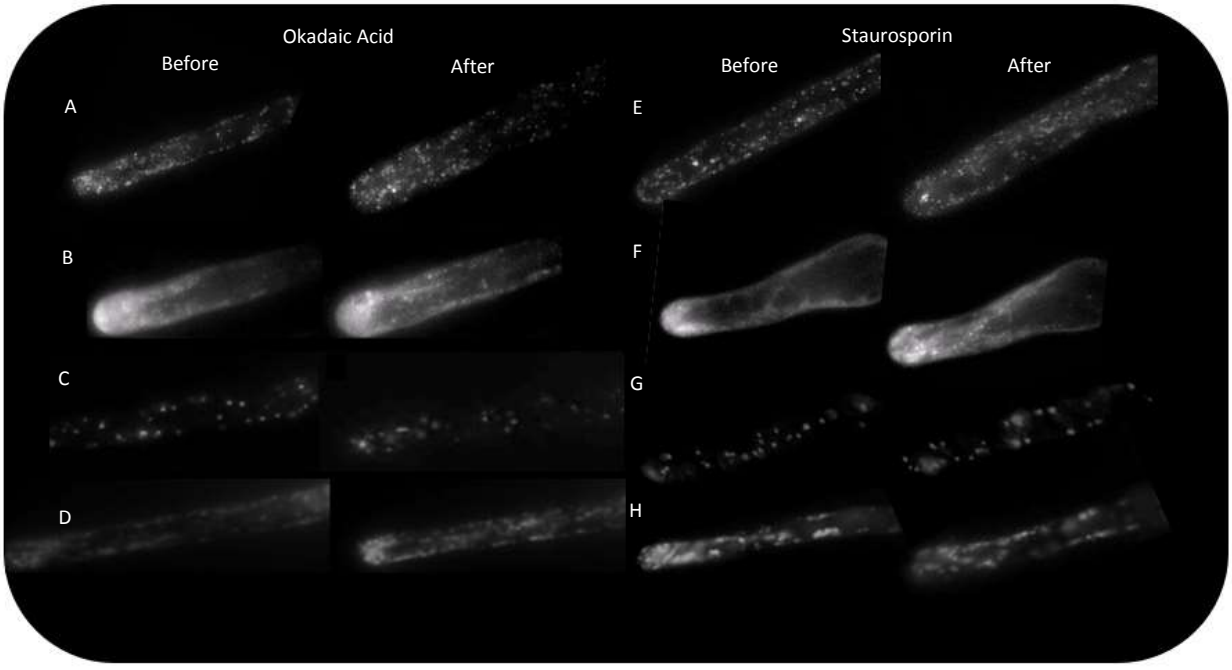

Figure 5: Comparison of organelle localization before and after administration of 200 nM okadaic acid (A, B, C, D) and staurosporin (E, F, G, H). The following letters designate each organelle. A, E: MYA1 myosin isoform. B, F: RabA4b vesicles. C, G: peroxisomes. D, H: Golgi bodies. Each picture is composed of a stack of images at different planes of the root hair at one time. No significant differences in signal strength or location were observed.

Organelle movements

Rationale: *If phosphorylation regulates movement, then changes in phosphorylation may lead to alteration in the average velocities of streaming organelles. Phosphorylation may also change the percentage of streaming organelles to stationary organelles instead of the velocities for every*

organelle.

MYA1 Movements

Observations of timelapse image sequences for myosin isoform MYA1 revealed an increase of velocities after staurosporin treatment and a decrease of velocities after okadaic acid treatment. However, only one data set was determined to have increased velocities (One-way ANOVA, p-value < 0.05) after eliminating all tracked velocities less than 0.5 μm/s (Figure 6A, B). These velocities were removed in this analysis to only consider organelles actively streaming. The normalized root hair average did not change from one, also indicating velocities above 0.5 μm/s were unaffected by inhibitors (Figure 6C). Individual root hairs before treatment had significant differences (One-way ANOVA, p-value < 0.001) among all root hair, supporting the general variability of these cells (Figure 6A, B). For staurosporin, the median was 0.83 μm/s (n = 1775) before treatment and 0.86 μm/s (n = 2021) after treatment (Figure 6). For okadaic acid, the median was 0.79 μm/s (n = 1358) before treatment and 0.78 μm/s (n = 875) after treatment. These numbers indicate that the average streaming velocities do not change significantly from either inhibitor.

For the proportion of streaming to stationary MYA1 signals for okadaic acid, three out of the four individual root hairs decreased in the amount of streaming signal by more than 15% (Figure 10A). For staurosporin, four out of the five individual root hairs increased in streaming signal by more than 15%, with one above 30% (Figure 10A). These percentages indicate that phosphorylation plays a role in MYA1 organelle movement through decreasing actively streaming MYA1 myosin, with unphosphorylated MYA1 having increased streaming signal (Figure 10F; t-test, p-value < 0.05).

RabA4b Movements

RabA4b vesicle movement was observed in timelapse image sequences as slightly increasing and decreasing velocity after treatment with inhibitors. However, the only significant individual data set treatment was for staurosporin, which increased in velocities (Figure 7A, B; One-way ANOVA, p-value < 0.05). All tracked velocities less than 0.5 µm/s were removed. The normalized root hair average did not change from one, indicating velocities above 0.5 µm/s were unaffected by inhibitors (Figure 7C). For staurosporin, the median was 0.79 µm/s (n = 1569) before treatment and 0.76 µm/s (n = 1570) after treatment. For okadaic acid, the median was 0.78 µm/s (n = 2008) before treatment and 0.79 µm/s (n = 2577) after treatment. Individual root hairs before treatment had significant differences (One-way ANOVA, p-value < 0.001) among all root hair, supporting the general variability of these cells (Figure 7A, B).

For the proportion of streaming to stationary RabA4b signals for okadaic acid, the six individual root hairs had inconsistent responses, with some increasing in ratio and others decreasing (Figure 10B). For staurosporin, similar results were obtained. Phosphorylation most likely plays an insignificant role in RabA4b vesicle movement based on the percentage of moving signals (Figure 10E, F; t-test, p-value > 0.05).

Golgi body Movements

Golgi body movements were observed to increase by okadaic acid while staurosporin was seen to be inconclusive in timelapse image sequences (Figure 8). From the graphs, individual root hairs treated with staurosporin were inconsistent in their responses, with one significantly increasing in velocities and another significantly decreasing (Figure 8B). Root hairs treated with okadaic acid significantly increased in movement (Figure 8A; One-way ANOVA, p-value < 0.05). For staurosporin, the median was 0.80 µm/s (n = 1735) before treatment and 0.79 µm/s (n

= 2050) after treatment. For okadaic acid, the median was 0.83 µm/s (n = 2500) before treatment and 0.86 µm/s (n = 2828) after treatment. The normalized root hair average did not change from one, indicating velocities above 0.5 µm/s were most likely unaffected by inhibitors (Figure 8C). Individual root hairs before treatment had significant differences (One-way ANOVA, p-value < 0.001) among all root hair, supporting the general variability of these cells (Figure 8A, B).

For the percentage of moving Golgi body signals for okadaic acid, three out of the four individual root hairs increased in the amount of moving signal by approximately 15% (Figure 10C). For staurosporin, individual root hairs were inconsistent in results, with two less than 10% different (Figure 10C). These ratios indicate that phosphorylated Golgi body organelles have an increased amount of Golgi body movement above 0.5 µm/s (Figure 10E; t-test, p-value < 0.05).

Peroxisome Movements

Peroxisome movement was observed to increase after treatment with staurosporin and okadaic acid. Individually, two data sets for okadaic acid significantly increased in velocity respectively, while one decreased (One-way ANOVA, p-value < 0.002). For individual staurosporin treatments, only one root hair significantly increased (One-way ANOVA, p-value < 0.05). All tracked velocities less than 0.5 µm/s were removed. For staurosporin, the median was 1.02 µm/s (n = 795) before treatment and 0.92 µm/s (n = 841) after treatment. For okadaic acid, the median was 0.84 µm/s (n = 2088) before treatment and 0.87 µm/s (n = 2502) after treatment (Figure 9). The normalized root hair average did not change from one, indicating velocities above 0.5 µm/s were unaffected by inhibitors (Figure 9C). Individual root hairs before treatment had significant differences (One-way ANOVA, p-value < 0.001) among all root hair, supporting the general variability of these cells (Figure 9A, B).

For the percentage of moving peroxisome signals for okadaic acid, three out of the four

individual root hairs increased in the amount of moving signal by more than 20% (Figure 10D). For staurosporin, three out of the four individual root hairs also increased in moving signal by approximately 15% (Figure 10D). These percentages, while not confirmed as significant, may indicate that phosphorylation plays a role in peroxisome organelle movement and is contradictory, with both inhibitors increasing actively moving peroxisomes (Figure 10E, F); t-test, p-value > 0.05).

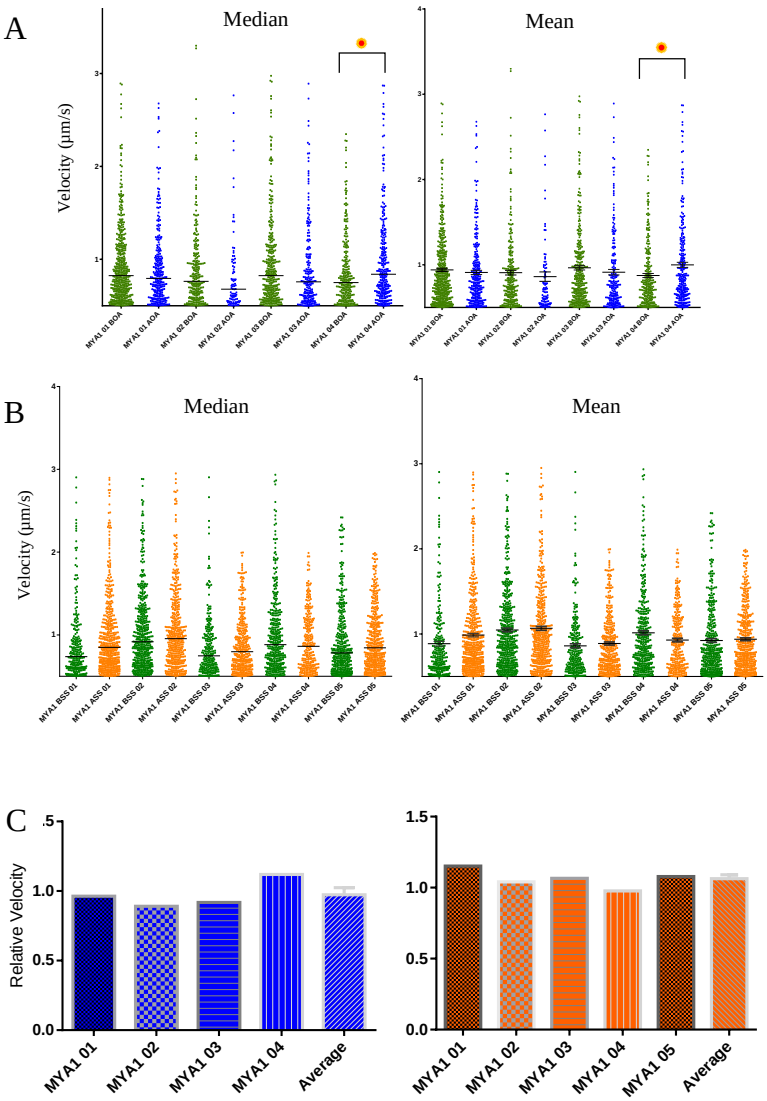

Figure 6: Velocities of MYA1 before and after administration of 200 nM okadaic acid (OA) and staurosporin (SS). Green dots indicate before inhibition, blue dots indicate after inhibition with OA, and orange dots indicate inhibition with SS. The graphs show the distribution of velocities above 0.5 µm/s in individual root hairs (A, B) with median and mean ± SEM indicated. Individual root hairs were also compared through a logarithmic cumulative distribution chart to determine whether individual velocity differences were significant (not shown). Additionally, root hairs were normalized (post-treatment ÷ pre-treatment) in order for the averages to be compared to 1, where post-treatment equals pre-treatment (C). Changes in individual velocities after OA and SS treatment were significant (+) only for OA4 (One-way ANOVA, p-value < 0.05). Normalized data was not significantly different from 1 for both okadaic acid and staurosporin (t-test, p-value > 0.05). SEM is less than 0.02.

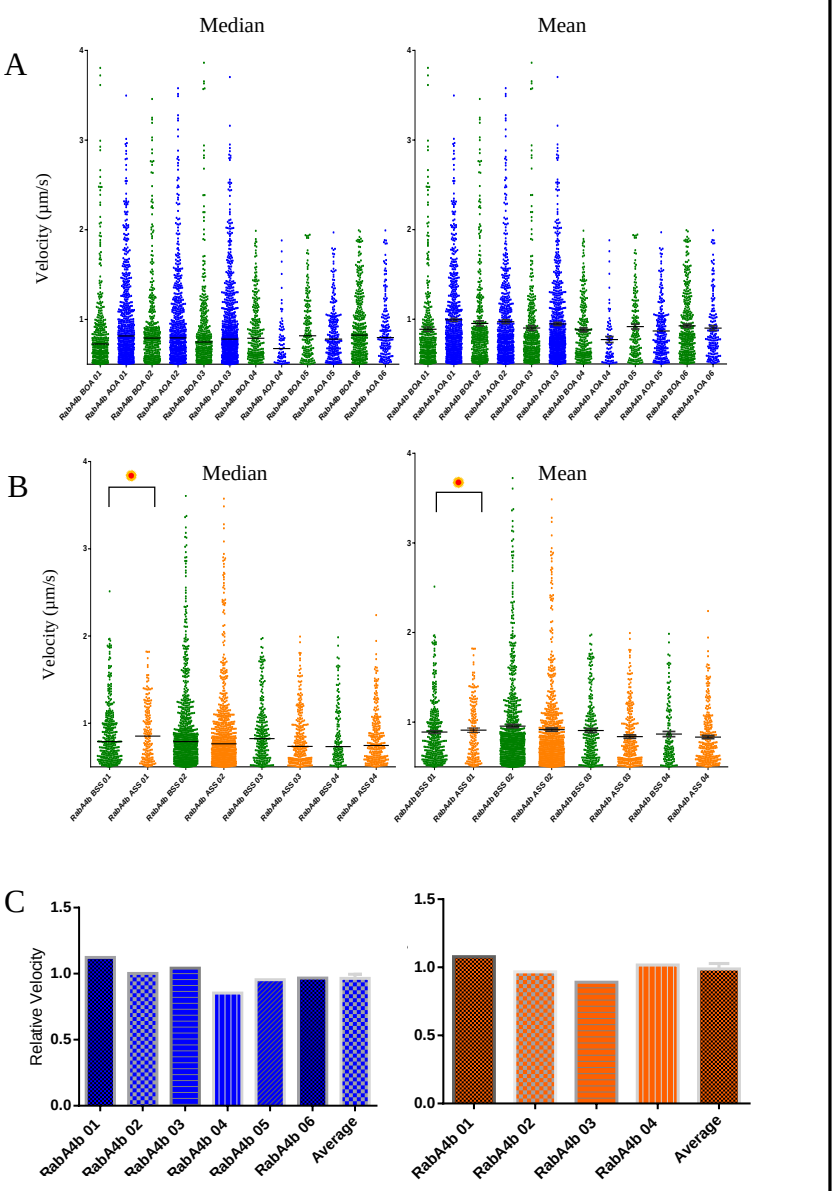

Figure 7: Velocities of RabA4b before and after administration of 200 nM okadaic acid (OA) and staurosporin (SS). Green dots indicate before inhibition, blue dots indicate after inhibition with OA, and orange dots indicate inhibition with SS. The graphs show the distribution of velocities above 0.5 µm/s in individual root hairs (A, B) with median and mean ± SEM indicated. Individual root hairs were also compared through a logarithmic cumulative distribution chart to determine whether individual velocity differences were significant (not shown). Additionally, root hairs were normalized (post-treatment ÷ pre-treatment) in order for the averages to be compared to 1, where post-treatment equals pre-treatment (C). The only individual velocity to significantly increase was SS1 (One-way ANOVA, p-value < 0.002). Normalized data was not significantly different from 1 for both okadaic acid and staurosporin (t-test, p-value > 0.05). SEM error bars are less than 0.02.

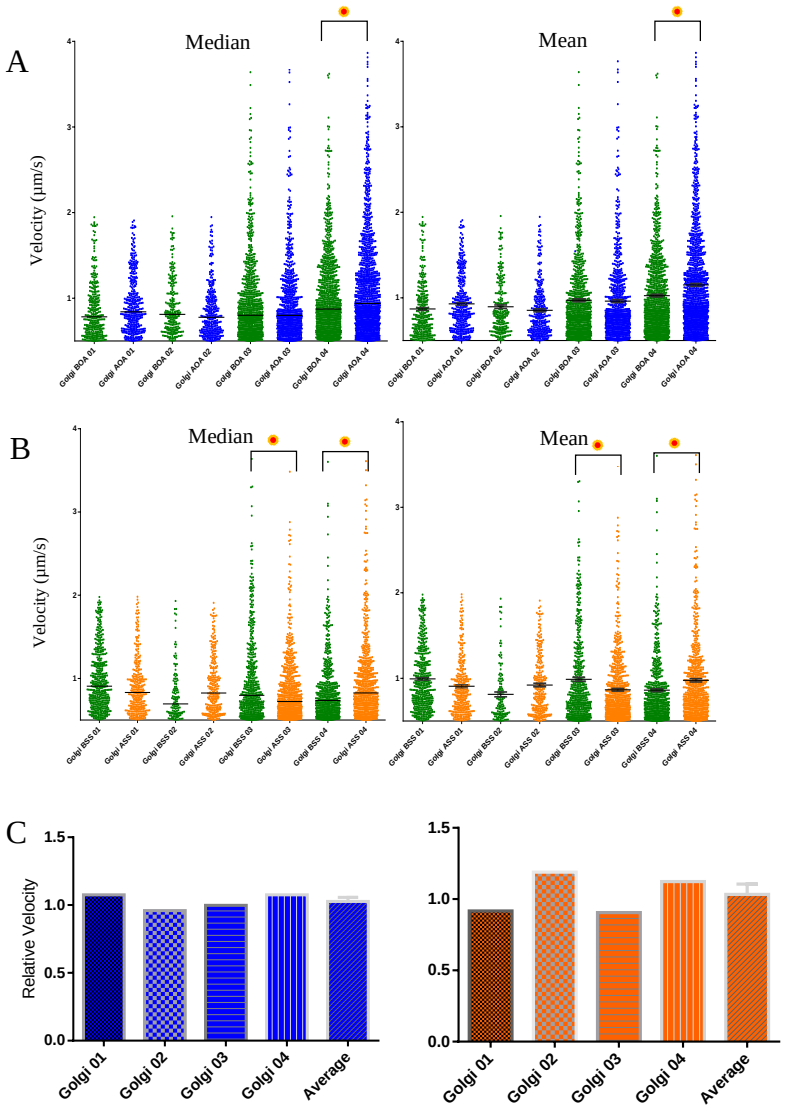

Figure 8: Velocities of Golgi bodies before and after administration of 200 nM okadaic acid (OA) and staurosporin (SS). Green dots indicate before inhibition, blue dots indicate after inhibition with OA, and orange dots indicate inhibition with SS. The graphs show the distribution of velocities above 0.5 µm/s in individual root hairs (A, B) with median and mean ± SEM indicated. Individual root hairs were also compared through a logarithmic cumulative distribution chart to determine whether individual velocity differences were significant (not shown). Additionally, root hairs were normalized (post-treatment ÷ pre-treatment) in order for the averages to be compared to 1, where post-treatment equals pre-treatment (C). For individual velocities, OA4 (+), SS3 (-), and SS4 (+) were shown to be significant changes in movement (One-way ANOVA, p-test < 0.05). Normalized data was not significantly different from 1 for both okadaic acid and staurosporin (t-test, p-value > 0.05). SEM error bars are less than

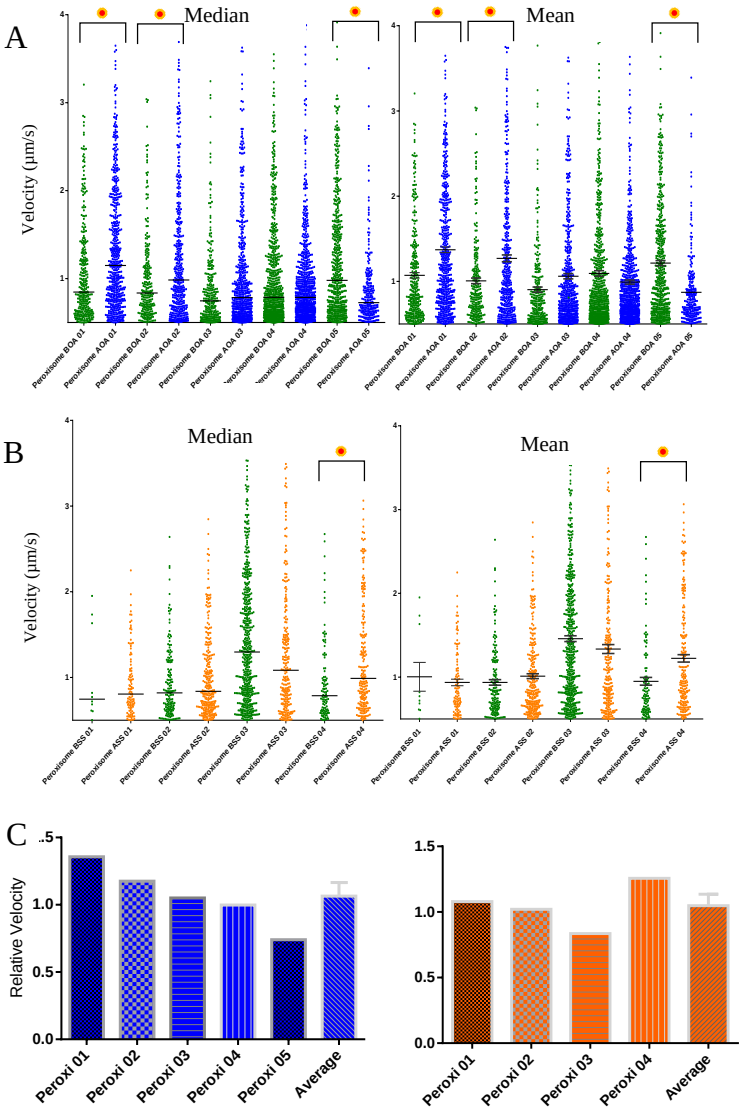

Figure 9: Velocities of peroxisomes before and after administration of 200 nM okadaic acid (OA) and staurosporin (SS). Green dots indicate before inhibition, blue dots indicate after inhibition with OA, and orange dots indicate inhibition with SS. The graphs show the distribution of velocities above 0.5 µm/s in individual root hairs (A, B) with median and mean ± SEM indicated. Individual root hairs were also compared through a logarithmic cumulative distribution chart to determine whether individual velocity differences were significant (not shown). Additionally, root hairs were normalized (post-treatment ÷ pre-treatment) in order for the averages to be compared to 1, where post-treatment equals pre-treatment (C). For individual velocities, peroxisomes OA1 (+), OA2 (+), OA5 (-), and SS4 (+) had significant differences in movement speed (One-way ANOVA, p-value < 0.05). Normalized data was not significantly different from 1 for both okadaic acid and staurosporin (t-test, p-value > 0.05). SEM error bars are less than 0.02.

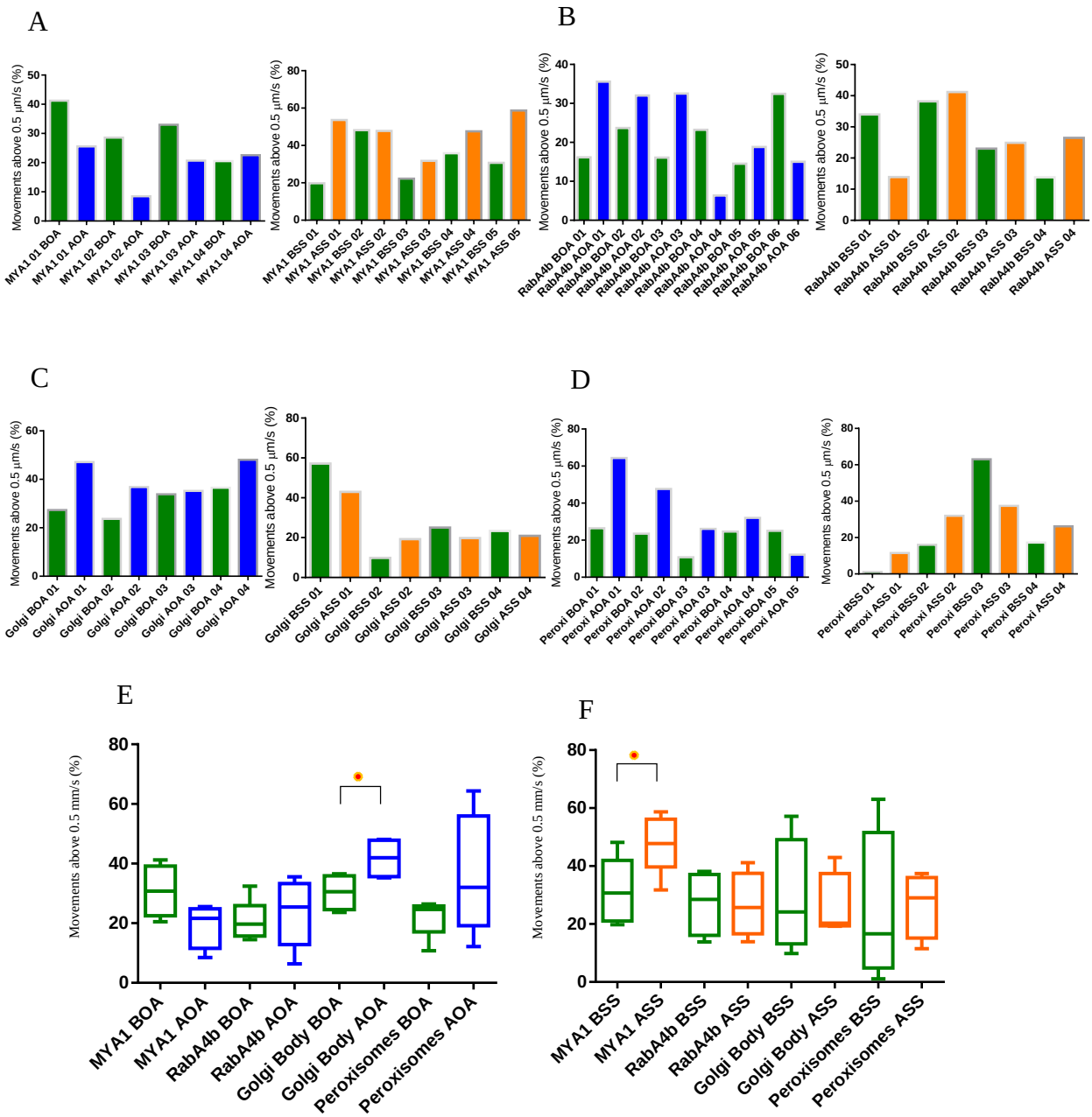

Figure 10: Comparison of all organelle velocities (A: MYA1, B: RabA4b, C: Golgi body, D: Peroxisomes) before and after administration of 200 nM okadaic acid (OA) and staurosporin (SS). Green bars indicate before inhibition, blue bars indicate after inhibition with OA, and orange bars indicate inhibition with SS. Each graph compares the percentage of movements above 0.5 µm/s before and after treatment with OA or SS. Box plots (E, F) of average percentages were included for statistical analysis. Golgi body treatment with okadaic acid average values was significant (t-test, p-value < 0.05). MYA1 treatment with staurosporin was also significant (t-test, p-value < 0.05). Okadaic acid treatment to MYA1 and peroxisomes also have clear trends. Inhibitors have effects on the percentage of movements above 0.5 µm/s, with organelles likely responding differently to the same inhibitors administered.

DISCUSSION

Phosphorylation affects the percentage of movements above stationary velocities

From initial data using kinase and phosphatase inhibitors, phosphorylation was strongly supported to affect myosin XI organelle trafficking, along with differences in the amount of change among different organelles. In particular, unphosphorylated MYA1 myosin isoform was supported to have greater movement than phosphorylated MYA1. The localization of organelle signal was never observed to change, supporting that phosphorylation does not halt myosin XI organelle trafficking, but serves as a regulator. Continued efforts to optimize the automated particle tracker and eliminate stationary particles have removed the previous increases or decreases in velocities above 0.5 μm/s after treatment of inhibitor. While individual root hairs and normalized data sets do have some significance in inhibitor treatments, these differences are not consistent toward a trend or pattern. Rather, the percentage of moving particles is the primary factor that is affected by phosphorylation, with changes present in the majority of organelle treatments. Specifically, MYA1 and Golgi bodies are supported to be regulated by phosphorylation, while RabA4b appears to be unaffected. Peroxisomes are also most likely affected by phosphorylation, but the fact that both okadaic acid and staurosporin increase the percentage of moving signals leads the results to be inconclusive until additional experiments are conducted, specifically to determine what effects these specific inhibitors have on peroxisomes. In general, phosphorylated Golgi bodies have an increased number of signals with active movement, while phosphorylated MYA1 becomes decreased in moving signals. The fact that phosphorylation does not always lead to increased movements may indicate phosphorylation differs in effect depending on the organelle or myosin.

Due to organelles being affected more by the general spectrum phosphatase inhibitor okadaic acid, further research with additional kinase and phosphatase inhibitors would assist in supporting whether these organelles are regulated by phosphorylation while being carried by myosin XI. Additional replications of all organelles could also be implemented in order to more accurately apply statistical analysis to the signal movement ratio graphs.

CONCLUSIONS

This experiment manipulated phosphorylation states in root hairs to determine whether myosin XI organelle trafficking is regulated by phosphorylation. From the following research, velocities that stream across the root hair are affected by phosphorylation in MYA1 myosin, Golgi bodies, and most likely peroxisomes. RabA4b vesicles, however, were not affected by phosphorylation. Phosphorylation also did not change localization of any of the organelles observed. Phosphorylation changes the amount of wiggling signals not actively moving, with phosphorylated organelles increasing or decreasing in moving signals. Future research could be done in using the actin control latrunculin to determine its effect on organelle movement. Novel ways of tracking diffuse or numerous signals such as endoplasmic reticulum, trans Golgi network, and mitochondria should also be sought after.

REFERENCES

Allen, R., Allen, N. (1978). Cytoplasmic streaming in ameboid movement. Annu. Rev. Biophys. Bioeng. **7,** 469-495.

Diet, A., Link, B., Seifert, G.J., Schellenberg, B., Wagner, U., Pauly, M., Reiter, W.D. and Ringli, C. (2006). The arabidopsis root hair cell wall formation mutant lrx1 is suppressed by mutations in the RHM1 gene encoding a UDP-L-Rhamnose synthase. Plant Cell. **18,** 1630-1641.

Dolan, L. (2006). Positional information and mobile transcriptional regulators determine cell pattern in the Arabidopsis root epidermis Journal of Experimental Botany **57,** 51-54.

Guimil, S., and Dunand, C. (2006). Patterning of Arabidopsis epidermal cells: epigenetic factors regulate the complex epidermal cell fate pathway. Trends in Plant Science **11,** 601-609.

Higashi-Fujimi, S., Ishikawa, R., Iwasawa, H., Kagami, O., Kurimoto, E., Kohama, K., Hozumi, T. (1995). The fastest actin-based motor protein from the green algae, *Chara*, and its distinct mode of interaction with actin. FEBS Lett. **375,** 151-154.

Ishida, T., Kurata, T., Okada, K., and Wada, T. (2008). A genetic regulatory network in the development of trichomes and root hairs. Annual Review of Plant Biology **59,** 365-386.

Kamiya, N., and Kuroda, K. (1956). Velocity distribution of the protoplasmic streaming in *Nitella* cells. Bot. Mag. Tokyo **69,** 544-555

Kersey, Y.M., Hepler, P.K., Palevitz, B.A., Wessells, N.K. (1976). Polarity of actin filaments in Characean algae. Proc. Natn. Acad. Sci. U.S.A. **73,** 165-167.

Ketelaar, T. (2013). The actin cytoskeleton in root hairs: all is fine at the tip. Current Opinion in Plant Biology **16,** 749-756.

Kwak, S.-H., and Schiefelbein, J. (2008). A Feedback Mechanism Controlling SCRAMBLED Receptor Accumulation and Cell-Type Pattern in Arabidopsis. Current Biology **18,** 19491954.

Kwak, S.-H., Shen, R., and Schiefelbein, J. (2005). Positional Signaling Mediated by a Receptor-like Kinase in Arabidopsis Science **307,** 1111-1113.

Kwak, S.-H., and Schiefelbein, J. (2007). The role of the SCRAMBLED receptor-like kinase in patterning the Arabidopsis root epidermis. Developmental Biology **302,** 118-131.

Lee, M.M., and Schiefelbein, J. (2002). Cell Pattern in the Arabidopsis Root Epidermis Determined by Lateral Inhibition with Feedback. Plant Cell **14,** 611-618.

Li, J.-F., and Nebenführ, A. (2007). Organelle targeting of myosin XI is mediated by two globular tail subdomains with separate cargo binding sites. The Journal of Biological Chemistry **282,** 20593.

Li J.F., Nebenführ A. (2008). The tail that wags the dog: The globular tail domain defines the function of myosin V/XI. Traffic **9,** 290–298.

Madison, S.L., and Nebenführ, A. (2013). Understanding myosin functions in plants: are we there yet? Current Opinion in Plant Biology **16,** 710-717.

Miller, D.D., De Ruikiter N.C.A., Bisseling, T., Emons, A.M.C. (1999). The role of actin in root hair morphogenesis: studies with lipochito oligosaccharide as a growth stimulant and cytochalasin as an actin perturbing drug. Plant J **17,** 141-154.

Morimatsu, M., Hasegawa, S., Higashi-Fuimi., S. (2002). Protein phosphorylation regulates actomyosin-driven vesicle movements in cell extracts isolated from green algae, *Chara coralline*. Cell Motil. Cytoshel. **53,** 66-76.

Nebenführ, A., Gallagher, L., Dunahay, T.G., Frohlick, J.A., Masurkiewitz, A.M., Meehl, J.B., Staehelin, L.A. (1999). Stop-and-go movements of plant Golgi stacks are mediated by acto-myosin system. Plant Physiol **121,** 1127-1141.

Odronitz, F., Kollmar, M. (2007). Drawing the tree of eukaryotic life based on the analysis of 2269 maually annotated myosins from 328 species. Genome Biol. **8,** R196.

Ojangu, E.-L., Järve, K., Paves, H., and Truve, E. (2007). Arabidopsis thaliana myosin XIK is involved in root hair as well as trichome morphogenesis on stems and leaves Protoplasma **230,** 193-202.

Park, E. (2010). Reverse genetic and cell biological approaches to the study of developmental functions of Class XI myosin in *Arabidopsis thaliana*. In Botany (Knoxville: University of Tennesse, Knoxville), pp. 161.

Park, E., **and Nebenführ, A.** (2011). Cytoskeleton and root hair growth. The Plant Cytoskeleton **2,** 259-275.

Park, E., **and Nebenführ, A.** (2013). Myosin XIK of *Arabidopsis thaliana* Accumulates at the Root Hair Tip and Is Required for Fast Root Hair Growth. *PLOS ONE* **8,** 76745.

Peremyslov V.V., Prokhnevsky A.I., Avisar D., Dolja V.V. (2008) Two class XI myosins function in organelle trafficking and root hair development in Arabidopsis thaliana. Plant Physiol **146,** 1109– 1116.

Peremyslov V.V., Prokhnevsky A.I., Dolja V.V. (2010) Class XI myosins are required for development, cell expansion, and F-Actin organization in Arabidopsis. Plant Cell **22,** 1883–1897.

Prokhnevsky, A.I., Peremyslov, V.V., and Dolja, V.V. (2008). Overlapping functions of the four class XI myosins in Arabidopsis growth, root hair elongation, and organelle motility. PNAS **105,** 19744-19749.

Redowicz, M.J. Regulation of nonmuscle myosins by heavy chain phosphorylation. J. Muscle Res. Cell Mot. **22,** 163-173.

Reichelt, S., Knight, A.E., Hodge, T.P., Baluska, F., Samaj, J., Volkmann, D., and Kendrick-Jones, J. (1999). Characterization of the unconventional myosin VIII in plant cells and its localization at the post-cytokinetic cell wall. The Plant Journal **19,** 555-567.

Rogers, S.I., Karcher, R.I., Roland, J.T., Minim A.A., Steffen, W., Gelfand, V.I. (1999). Regulation of melanosome movement in the cell cycle by reversible association with myosin V. J. Cell Biol. **146,** 1265-1276.

Sbalzarini, I.F. and Koumoutsakos, P. (2005). Feature point tracking and trajectory analysis for video imaging in cell biology. J. Struct. Biol. **151,** 182–195.

Sellers, J.R. (2000). Myosins: a diverse superfamily. BBA **1496,** 3-22.

Schiefelbein, J. (2003). Cell-fate specification in the epidermis: a common patterning mechanism in the root and shoot Cell-fate specification in the epidermis: a common patterning mechanism in the root and shoot. The Plant Cell **6,** 74-78.

Schiefelbein, J.W., Masucci, J.D., and Want, H. (1997). Building a Root: The Control of Patterning and Morphogenesis during Root Development. The Plant Cell **9,** 1089-1098.

Shimmen T. (2007). The sliding theory of cytoplasmic streaming: Fifty years of progress. J. Plant Res. **120,** 31–43.

Shimmen T., Yokota E. (1994). Physiological and biochemical aspects of cytoplasmic streaming. Int. Rev. Cytol. **155,** 97–139.

Tominaga, M., Kimura, A., Yokota, E., Haraguchi, T., Shimmen, T., Yamamoto, K., Nakano, A., Ito, K. (2013). Cytoplasmic streaming velocity as a plant size determinant. Dev. Cell **27,** 345-52.

Tominaga M., Kojima H., Yokota E., Orii H., Nakamori R., Katayama E., Nason M., Shimmen T., Oiwa K. (2003) Higher plant myosin XI moves processively on actin with 35 nm steps at high velocity. EMBO J. **22,** 1263–1272.

Tominaga M., Kojima H., Yokota E., Nakamori, R., Anson, M., Shimmen, T., Oiwa, K. (2012). Calcium-induced mechanical change in the neck domain alters the activity of plant myosin XI. J Biol Chem. **287,** 30711-30718.

Tominaga, M., Morita, K., Sonobe, S., Yokota, E., and Shimmen, T. (1997). Microtubules regulate the organization of actin filaments at the cortical region in root hair cells of hydrocharis. Protoplasma **199,** 83-92.

Tominaga, M., Yokota, E., Sonobe, S., and Shimmen, T. (2000). Mechanism of inhibition of cytoplasmic streaming by a myosin inhibitor, 2,3-butanedione monoxime. Protoplasma **213,** 46- 54.

Trybus, K.M. (1991). Regulation of smooth muscle myosins. Cell Motil Cytoskel **18,** 81-85.

Vick, V.K., and Nebenführ, A. (2012). Putting On The Breaks: Regulating Organelle Movements in Plant Cells. JIPB **54,** 868-874.

Vidali, L., Burkart, G.M., Augustine, R.C., Kerdavid, E., Tüzel, E., Bezanilla, M. (2010). Myosin XI is essential for tip growth in *Physconmitrella patens.* Plant Cell **22,** 1868-1882.